Journal of Materials Chemistry B

Accepted Manuscript

ROYAL SOCIETY OF CHEMISTRY

www.rsc.org/materialsB

Cite this: DOI: 10.1039/c0xx00000x

www.rsc.org/xxxxxx

ARTICLE TYPE

Perylene Derivatives Bridged Au-Graphene Nanohybrid for Label-Free HpDNA Biosensor

Wei Zhang, Fenghua Li*, Yuwei Hu, Shiyu Gan, Dongxue Han, Qixian Zhang, Li Niu*

Received (in XXX, XXX) XthXXXXXXXXX 20XX, Accepted Xth XXXXXXXXX 20XX

DOI: 10.1039/b000000x

Along with the challenges of wet-chemically preparing graphene based nanohybrids, for example, easy aggregation, low-stability in solution environment and insufficient loading amount, here, we report the preparation and application of a type of π-conjugated molecules, perylenetetracarboxylic acid di-imide (PDI) functionalized graphene material with high density of gold nanoparticles (AuNPs). In this nanohybrid, the PDI molecule comprises five-connected benzene rings and positively charged terminals composed of two symmetrical imidazole rings and amine groups, which offers the intrinsic driving force for π-π interactions with graphene and also serves as the active sites for immobilization of AuNPs. Transmission electron microscopy results demonstrated that AuNPs were uniformly dispersed and densely covered on the PDI functionalized graphene compared to the control experiment without PDI. To prove its biological application, the Au-PDI-graphene nanohybrid was chosen as a sensing material for fabricating a label-free electrochemical impedance hairpin DNA (hpDNA) biosensor for detection of human immunodeficiency virus 1 gene. When hpDNA was hybridized, it exhibited a sensitive electrochemical impedance variation on the Au-PDI-graphene modified electrode. This fabricated hpDNA biosensor reveals a wide linear detection range and a relative low detection limit. Thanks to high stability and efficient electrochemical impedance sensitivity, this nanohybrid would offer a broad range of possible DNA sequence for specific applications in biodiagnostics and bionanotechnology.

Introduction

Graphene featured in large flat surface area, high electron conductivity and good electron acceptor, which make it become an excellent candidate in extensive applications such as sensors,[1] drug delivery[2] and disease diagnosis.[3] For example, the large flat surface area can load large quantity of biomolecules,[4] drugs[2] and nanoparticles.[5] Another typical characteristic of π–conjugated structure plays not only a non-covalent functionalization platform (π-π interaction), but also acts as a good energy/electron acceptor for high-rate fluorescence quenching that can be used for fluorescence-ultrasensitive sensors.[1] Among numerous efforts devoted to graphene preparation, most of them are derived from graphene oxide (GO) by wet-chemical methods using strong reduction reagents such as hydrazine,[6] $NaBH_4$[7] and ascorbic acid. However, graphene in a large quantity made by this direct reduction often results in irreversible agglomerates because of strong π–π stacking interactions between individual graphene sheets. Additionally, graphene itself lacks specific functionality (e.g., molecule or target recognition), which hinders its further applications in various fields.

Nanoparticles are usually integrated onto graphene for promotion of graphene multifunction, for example, for enhancing sensitivity and lowering the detection limit in biosensors,[5] and for introducing catalysis functionality in photo- and electro-catalysis.[8] Generally, nanohybrids of metal nanoparticles decorated graphene are fabricated through one-step reduction method in the presence of both precursors of graphene and metal nanoparticles.[9] However, the aggregation trend of graphene in solution causes a low-loading amount of nanoparticles and non-uniform dispersion and relatively low stability. To overcome these drawbacks, tailoring graphene through covalent and non-covalent interactions[10] is impressively demonstrated as an effective strategy to improve graphene solution properties. For instance, polymers and other molecules were attached upon the graphene sheets through covalent binding to stabilize graphene.[11] These modification molecules were highly hydrophilic and possessed coupling groups which could covalently reacted with graphene. However, if we can introduce the modification molecules with multifunction, such as dispersion ability, nanoparticles loading sites and even recognition that would broaden graphene in more complex and advanced applications.

In this paper, we report a bifunctional perylenetetracarboxylic acid di-imide (PDI) (molecular structure shown in Fig. 1a) to non-covalently modificate graphene. This molecule is comprised of a five-connected benzene ring (core) and two positive side chains (arms) in which the core plays a role in π-π interacting with graphene and the arm acts as a bridge to graft gold nanoparticles (AuNPs). The resulted PDI-graphene exhibits good water dispersion and successfully loads uniformly-dispersed and dense AuNPs. DNA analysis was taken as an example to prove a

biological application. A simple label-free impedance DNA biosensor was fabricated for detection of human immunodeficiency virus 1 (HIV-1) pol gene sequence. We choose hairpin DNA (hpDNA) as the probe of DNA biosensor because of high specificity for hybridization to target sequence. The results demonstrate the sensing material of Au-PDI-graphene shows a high sensitivity to DNA detection and mismatch recognition.

Experiment section

Synthesis of GO, graphene and PDI

GO was prepared by oxidizing natural graphite powder (320 mesh) based on modified Hummers method.[12] As-prepared GO was dispersed in ultrapure water by using ultrasonication to obtain a brown dispersion. Then it was subjected to dialysis for 4 days to completely remove residual salts and acids. The resulting purified GO powder was collected by centrifugation and air-dried. GO powder was redispersed in ultrapure water to create a 0.05 wt% dispersion. Then the dispersion was exfoliated through ultrasonication for 1 hour, and the bulk GO powder was transformed into GO nanoplates. Graphene was obtained by chemical reduction of GO. Briefly, 20 mL GO aqueous suspension (0.05 wt%) was mixed with 20 mL ultrapure water in a 100 mL glass vial and then 0.012 mL hydrazine solution (50% in water) was introduced. Subsequently, few drops of ammonia solution (25% in water) were added to adjust the mixture pH to 10. After vigorously stirring for minutes, GO nanosheets were reduced to graphene nanoplates under refluxing the mixture for 30 minutes in an oil bath (95 °C). The final product was then filtered through a Nylon membrane (0.22 μm pores), washed, and dispersed in 50 mL ultra-pure water. The red PDI powder was fabricated according to our previous report.[13]

Au-PDI-graphene platform fabrication

PDI-graphene nanohybrid was fabricated as following. 1 mg PDI was added into graphene aqueous suspension (0.008 wt%, 20 mL). The obtained red mixture was then ultrasonicated for 30 minutes and stirred overnight at 40 °C. Subsequently, the product was filtered through a Nylon membrane (0.22 μm pores) to remove unbound PDI molecules, thoroughly washed and dispersed in 20 mL water. The obtained solution was used to prepare Au-PDI-graphene nanocomposite. The citrate stabilized AuNPs were prepared following Gao's work.[14] Briefly, 0.165 mL of 0.03 M $HAuCl_4 \cdot 3H_2O$ aqueous solution and 0.5 mL of 0.01 M trisodium citrate solution was added to 13.335 mL water in a conical flask. Then, ice-cold 6 mL of 0.01 M $NaBH_4$ solution was added dropwise with constant stirring. Finally, the resulted wine colored solution was stored at 4 °C for the following use. Then 10 mL of AuNPs solution prepared in the previous section was transferred to 10 mL PDI-graphene with constant stirring for 20 hours at room temperature. Finally, the product was filtered, washed and dispersed in 10 mL water. As a control experiment, 10 mL of the AuNPs solution was transferred to 10 mL graphene solution (0.008 wt%) with the absence of PDI to prepare Au-graphene nanocomposite.

HpDNA immobilization and hybridization

Typically, the glass carbon electrode (GCE) was polished using 1, 0.3, 0.05 μm Al_2O_3 slurry respectively and washed ultrasonically with ethanol and water separately. An aliquot of 5 μL Au-PDI-graphene solution was pipetted onto the GCE surface using a microsyringe. After dried, the hpDNA solution (70 μL, 1.0×10^{-6} M) was applied to the Au-PDI-graphene/GCE surface and incubated for 12 hours at room temperature. Next, the electrode was washed with sodium dodecylsulfate (SDS) solution (0.2%) and ultrapure water to remove unattached hpDNA probe.

DNA hybridization reaction was conducted by dropping appropriate concentration of target DNA solution (5 μL) onto the hpDNA probe surface and kept the electrode at 37 °C for 45 minutes. The hybridization scheme is shown in Fig. 1b. Then the electrode was washed with SDS solution (0.2%) to further remove un-hybridized DNA. The same procedure as mentioned above was applied to the probe-modified electrode for hybridization with single-base mismatched DNA sequences.

Results and discussion

The overall procedure including the preparation of Au-PDI-graphene platform, hpDNA immobilization and detection of target DNA employing electrochemical impedance spectroscopy (EIS) as a label-free technique is illustrated in Fig. 1b. Subsequently, the main experimental observations with broad discussions are presented.

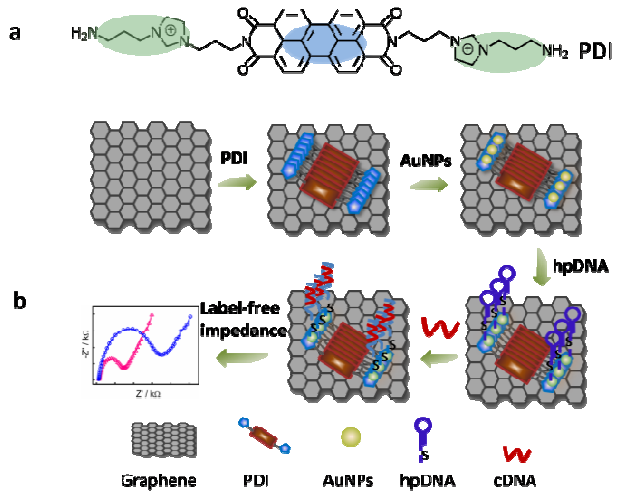

Fig. 1 The molecular structure of PDI (a), schematic representation of Au-PDI-graphene nanohybrid fabrication and hpDNA hybridization detection (b).

Synthesis and characterization of PDI-graphene

Graphene was obtained by wet-chemical reduction of GO using hydrazine with the solution colour changing from yellow to dark brown (Fig. 2a, inset). And the absorption band red-shifted from 230 nm to 268 nm in ultraviolet-visible (UV-Vis) spectrum(Fig. 2a, dash dot dot), which may be stemmed from the restored π-network.[15] The X-ray photoelectron spectrum (XPS) results also demonstrated the formation of graphene (Fig. S3a† and b†). Morphology of large graphene sheet was observed by transmission electron microscopy (TEM) and the sheet size was

found to be a few micrometers (Fig. 3a). The large graphene sheet could offer sufficient basal plane for the subsequent anchoring of PDI.

PDI molecule consists of five-connected benzene rings and positively charged terminals including two symmetrical imidazole rings and amine groups (Fig. 1a). It dispersed well in water and formed pink solution (Fig. 2a, inset). The five-connected benzene rings offer the intrinsic driving force for π-π interactions between PDI and graphene sheets; the solvophilic imidazole rings and amine groups made PDI-graphene hybrid more hydrophilic than graphene. The formed PDI-graphene hybrid solution displayed a pale violet red color (shown in Fig. 2a, inset). Due to the π-π stacking interaction between perylene unit and graphene sheets, the two absorption peaks of PDI around 543 and 500 nm shifted to 563 and 512 nm in PDI-graphene nanohybrid (Fig. 2a, solid). No absorption peak of graphene was observed at around 500 nm (Fig. 2a, dash dot dot). On the other hand, the aggregation state of PDI on graphene sheets is crucial for understanding the self-assembly on graphene. Perylene molecules were often in the form of aggregation state in aqueous solution, which could be explained by UV-Vis absorption spectra. The absorption ratio of the 0 → 0($A^{0\rightarrow 0}$) (543 nm) to the 0 → 1 ($A^{0\rightarrow 1}$)(500 nm) transition was directly related to the degree of perylene aggregation.[13,16] Hence, the degree of PDI molecule aggregation could be illustrated by the value of $A^{0\rightarrow 0}/A^{0\rightarrow 1}$ and a higher value indicated a lower degree of aggregation among perylene derivatives.[17] The high $A^{0\rightarrow 0}/A^{0\rightarrow 1}$ value (0.60) further validated that PDI molecules were successfully anchored onto graphene sheets and have a lower aggregation degree on graphene sheets comparing with that of pure PDI (0.47) (Fig. 2a). In XPS, an exclusive single peak at 400.0 eV (Fig. 2b, inset) was also observed, which was assigned to the quaternary N coordination.[18] These characteristics confirmed the presence of PDI in PDI-graphene hybrid. And from the XPS, the mass of PDI was generally estimated to be 1.6 mg per mg graphene.

Upon the anchoring of PDI to graphene, the FTIR spectra of GO, graphene, PDI and PDI-graphene were investigated (Fig. 2c and S1†). The characteristic peaks were summaried in Table S1, which provided further evidence for the formation of PDI-graphene nanohybrid. Additionally, fluorescence emission spectra of PDI and PDI-graphene nanohybrid were also recorded. As our previous work reported, the strong fluorescence of PDI was quenched by the addition of graphene.[13] (Fig. 2d).

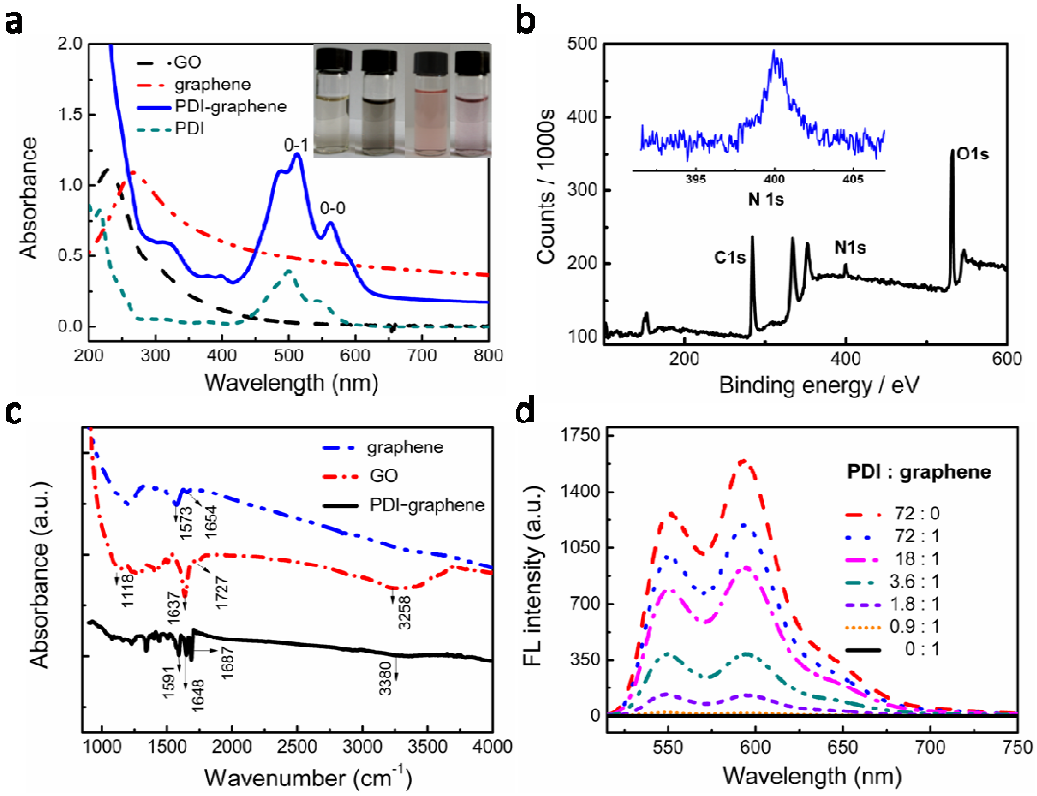

Fig. 2 (a) UV-vis absorption spectra of GO(dash), graphene (dash dot dot), PDI-graphene (solid), PDI (short dash); inset: photographs of GO (left), graphene (brown), PDI (pink), PDI-graphene (right) solutions; (b) XPS spectra of PDI-graphene. Inset: the N1s spectrum; (c) FTIR spectra of graphene (dash dot dot), GO (dash dot), and PDI-graphene (solid); (d) Fluorescence emission spectra of aqueous solutions of PDI, graphene and PDI-graphene nanohybrid with different graphene concentration at λ_{exc} = 491 nm.

Cite this: DOI: 10.1039/c0xx00000x

www.rsc.org/xxxxxx

ARTICLE TYPE

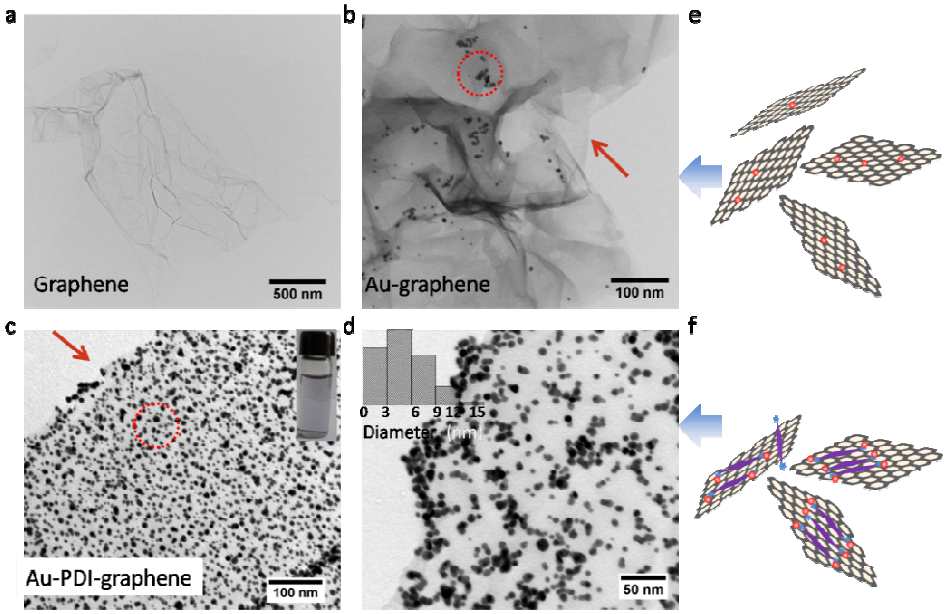

Fig. 3 TEM images of graphene (a), Au-graphene (b), Au-PDI-graphene at low magnification (c) and high magnification (d). Inset: the photograph of Au-PDI-graphene dispersions in ultrapure water (c) and the AuNPs size distribution obtained from measuring 400 randomly selected particles (d). Schematic illustration of the proposed structures of Au-graphene (e) and Au-PDI-graphene nanohybrid (f).

AuNPs loading on PDI-graphene nanosheets

The AuNPs were dispersed in water resulting in bright wine colored solution (Fig. S2a†, inset). And well-dispersed AuNPs with uniform diameter were observed in TEM image (Fig. S2a† and b†). The electrostatic repulsion among citrate anions in the outer layer of AuNPs were beneficial to the dispersion of the AuNPs. The UV-Vis characteristic absorption peak of AuNPs was at ca. 516 nm (Fig. S2c†). The wine colored AuNPs solution was then added into PDI-graphene solution and stirred for 20 hours, the colour of solution became lavender, showing the formation of Au-PDI-graphene nanocomposite (Fig. 3c, inset).

The surface charge of nanomaterial is very important for defining the composition of the formed nanohybrid. The zeta potential measurement gave the information of surface charge of the nanomaterial and was used to detect positively charged PDI and negatively charged AuNPs binding to graphene sheets as this would change the overall surface charge.[19] The graphene diluted by water resulted in a zeta potential value of ~ -19.4 mV, ascribed to surface carboxylic acid group. When graphene sheets were modified by PDI, their zeta potential significantly increased up to about 8.50 mV. It is the reason that the positive charge of PDI counters balance the negative charge of graphene. Furthermore, the negatively charged AuNPs accounted for the zeta potential value of -1.82 mV for Au-PDI-graphene nanohybrid.

The surface electronic composition of the nanohybrid was studied by XPS. In Au-PDI-graphene hybrid, the XPS signature of the Au 4f doublet ($4f_{7/2}$ and $4f_{5/2}$) of the resulting AuNPs was represented in Fig. S3c†. The Au $4f_{7/2}$ and $4f_{5/2}$ peaks appeared at *ca*. 83.5 and 87.1 eV (peak to peak distance of 3.6 eV), respectively, which were consistent with the Au^0 state.[19b] It confirmed the presence of AuNPs in Au-PDI-graphene hybrid.

Pure graphene sheets with few carboxyl groups on the edge made it difficult to modify citrate protected AuNPs. Relatively small density of AuNPs were dispersed on graphene sheets and most of them aggregated (Fig. 3b). However, the integration of positively charged PDI turned it around as observed in TEM (Fig. 3c). After PDI functionalization, the AuNPs covered the most part of PDI-graphene sheets surface and were uniformly dispersed. A size-distribution histogram was obtained from measuring 400 randomly selected particles (Fig. 3d, inset). The mean diameter was estimated to be *ca*. 6 nm. The surface area of AuNPs was calculated to be 51.8 m^2/g using the following Equation (1) :

$$S = \frac{6000}{\rho d} \quad (1)$$

Where d is the mean diameter (nm, TEM result), S is the surface area (m^2/g), and ρ represents the density of Au (19.32 g/cm^3). This large surface area and high loading capacity of AuNPs provided great potential for biomolecule immobilization.

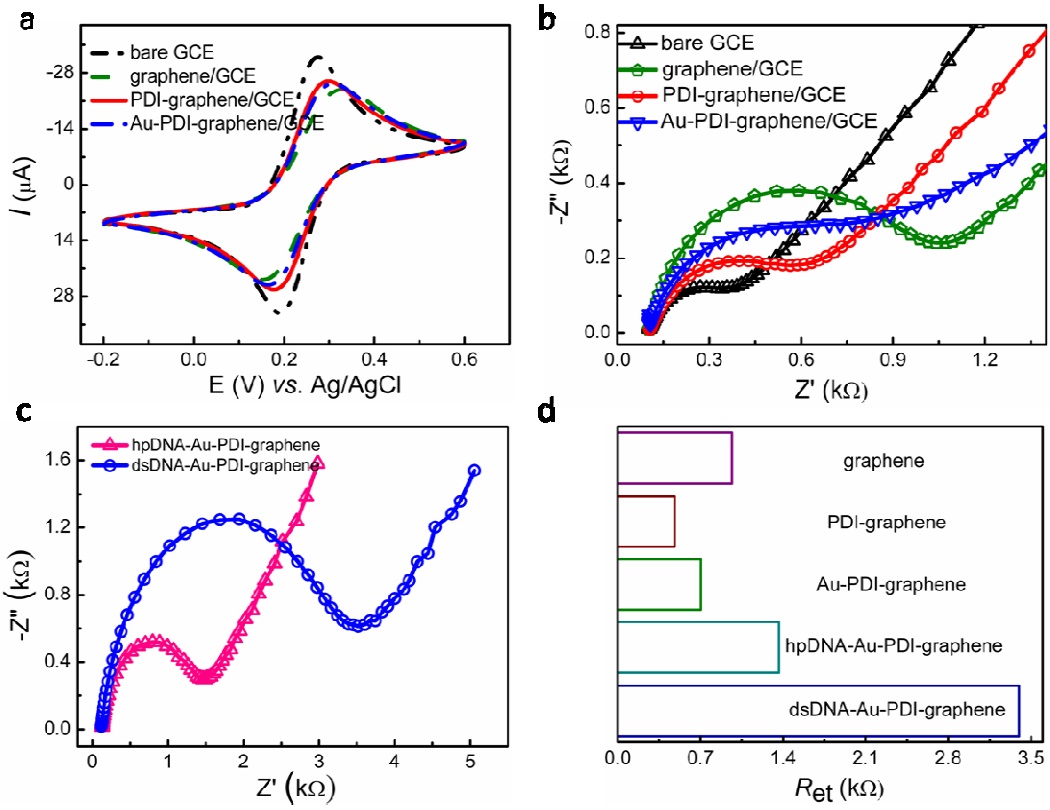

Fig. 4 (a) Cyclic Voltammograms recorded at bare GCE (dash dot dot), graphene/GCE (dash), PDI-graphene/GCE (solid) and Au-PDI-graphene/GCE (dash dot) in 2.0 mM $[Fe(CN)_6]^{3-/4-}$(1:1) solution containing 0.1 M KCl. (b) Nyquist diagrams obtained at bare GCE (Δ), graphene/GCE (⌓), PDI-graphene/GCE (○) and Au-PDI-graphene/GCE (▽) in 2.0 mM $[Fe(CN)_6]^{3-/4-}$(1:1) solution containing 0.1 M KCl. (c) Nyquist diagrams recorded at hpDNA-Au-PDI-graphene/GCE (Δ) and after hybridization with its complementary sequences (○). The detection concentrations of these sequences were selected as 1.0×10^{-10} M. (d) The R_{et} value of graphene/GCE, PDI-graphene/GCE, Au-PDI-graphene/GCE, hpDNA-Au-PDI-graphene/GCE, dsDNA-Au-PDI-graphene/GCE shown in histogram.

Fundamental electrochemical properties of Au-PDI-graphene nanohybrid modified electrode

To perform electrochemical measurement, an aliquot of graphene, PDI-graphene and Au-PDI-graphene solution was pipetted onto the GCE surface using a microsyringe, respectively and dried at room temperature.

Although graphene were well-known for their high electronic conductivity, the cyclic voltammograms (CVs) shown in Fig. 4a revealed that graphene impeded the electron transfer of $[Fe(CN)_6]^{3-/4-}$, due to the negatively charged carboxylic groups on graphene sheets.[20] Compared to graphene, PDI-graphene displayed a faster electron transfer rate, because the introduction of PDI led to an increase of the redox probe to the electrode surface. Subsequently, lower redox current and more sluggish electron transfer behavior of $[Fe(CN)_6]^{3-/4-}$ were observed on Au-PDI-graphene modified electrode (Fig. 4a), indicating that negatively charged AuNPs prevented $[Fe(CN)_6]^{3-/4-}$ from reaching the electrode surface.

EIS could sensitively response to subtle change of the electrode-solution interface.[21] Once the electrode-solution interface was altered, the electron transfer resistance (R_{et}) would change correspondingly. And it also provides the feasibility to evaluate the electrochemical properties of Au-PDI-graphene platform. The Nyquist plots of $[Fe(CN)_6]^{3-/4-}$ at the graphene, PDI-graphene and Au-PDI-graphene modified GCE were shown in Fig. 4b, respectively. The diameter of semicircle at high frequencies stands for R_{et}. Their R_{et} values were in the order: PDI-graphene (481 Ω) < Au-PDI-graphene (702 Ω) < graphene (967 Ω). These observations were consistent with the CV results (Fig. 4a). And these electrochemical results demonstrated that Au-PDI-graphene hybrid equipped with the good electron transfer kinetics, which was well suited for electrochemical biosensing.

Application

As Au-PDI-graphene platform offered the advantages such as large surface area and exceptionally high electron conductivity, these superior properties have laid solid basis for further incorporating DNA probe as biosensing devices, which is addressed below with hpDNA as an example.

Thiolated hpDNA was immobilized on the AuNPs *via* strong Au-S bonding resulting in a relatively packed monolayer, which repelled $[Fe(CN)_6]^{3-/4-}$ and led to an increase in R_{et} value. Thus, the hpDNA-Au-PDI-graphene modified electrode had a larger R_{et} (1365 Ω) than that of the Au-PDI-graphene platform modified

electrode (702 Ω) (Fig. 4b and c). After hpDNA hybridization with complementary DNA (cDNA), an increased R_{et} value (3400 Ω) was observed (Fig. 4c, ○), indicating the formation of duplex DNA. With the formation of duplex DNA, the thickness of DNA film increased,[21c] and the number of negative charges went up. It was much more difficult for $[Fe(CN)_6]^{3-/4-}$ to reach the electrode surface. Consequently, the R_{et} value increased following the formation of dsDNA. And the R_{et} value changed for every modification on electrode is graphically shown by histogram in Fig. 4d.

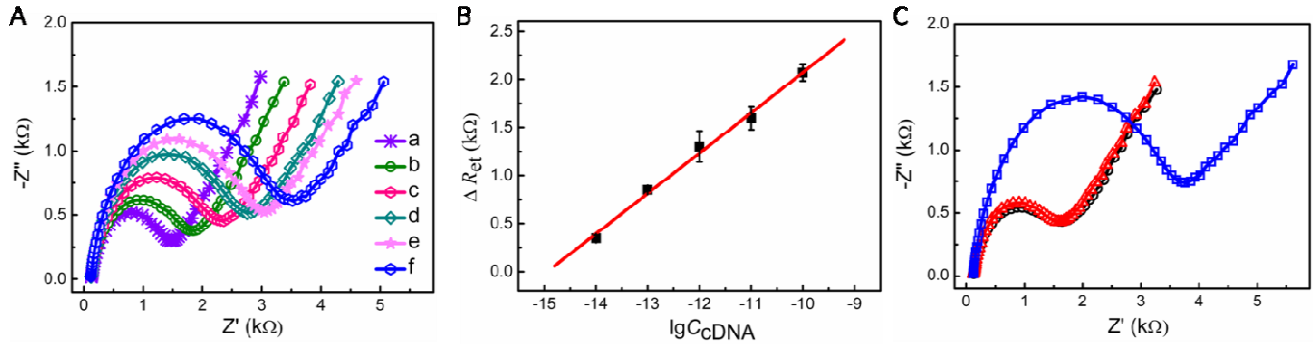

Fig. 5 (A) Nyquist diagrams recorded at hpDNA immobilized Au-PDI-graphene platform modified GCE (a) and after hybridization with its complementary sequences of different concentrations: 1.0×10^{-14}, 1.0×10^{-13}, 1.0×10^{-12}, 1.0×10^{-11} and 1.0×10^{-10} M (b-f), (B) The plot of ΔR_{et} *vs*. the logarithm of complementary sequences concentrations; (C) Nyquist diagrams recorded at hpDNA-Au-PDI-graphene/GCE (○) and after hybridization with its complementary sequences (□) and one-base mismatched sequences(Δ).

The relation between impedance signal change and concentration of cDNA was investigated as shown in Fig. 5A. The R_{et} value increased with the increase of cDNA concentration. And the difference (ΔR_{et}) in the electron transfer resistance before and after hybridization was adopted as the measurement signal. The ΔR_{et} value was linear with the logarithm of the cDNA concentration at the range from 1.0×10^{-14} to 1.0×10^{-10} M. Its regression equation was ΔR_{et} = 419.06lg*C*+6260.3 with the regression coefficient (γ) 0.9910 (Fig. 5B).When $C_{cDNA} > 1.0\times10^{-10}$ M, a plateau was reached and no obvious change in R_{et} was found with the increase of the target concentration. In this article, the detection limit was calculated to be 1.2×10^{-15} M with 3σ (where σ was the relative standard deviation of 11 parallel measurements of blank solution). It means that the fabricated hpDNA biosensor shows highly sensitive detection performance.

In addition, compared with other platforms based on graphene (Table S2), the proposed platform has higher efficiency with lower detection limit and relatively wider detection range.

The selectivity of hpDNA sensing platform has been validated by performing hybridization measurement with 1×10^{-10} M single-nucleotide mismatched DNA sequence. There is no obvious change in R_{et} value after hybridized with single-base mismatched sequence comparing to probe immobilized platform (Fig. 5C). This observation validates a very high selectivity for the target sequence, which is consistent with previously reported results where hpDNA sensor exploited low hybridization temperature and high probe density.[22] The high-selectivity of hpDNA biosensor stemmed from the stem-loop structure,[22-23] and low hybridization temperature (37 °C). Hybridization dynamics could be used to illustrate it. The dynamics of the hpDNA is dependent on the stability of the stem, which is closely associated with temperature. At the melting temperature of the hpDNA (~44 °C), half of the base pairs are generally broken and the stem is destabilized. So, when hybridization temperature is close to the melting temperature of the hpDNA, its secondary structure is deteriorated, and subsequently the selectivity is lost.[22] In addition, in this platform, well-dispersed AuNPs with high loading capacity and their large surface to volume ratio offer a potential to high probe density and make it possible for excellent selectivity. If the probe density decreases, the selectivity also decreases correspondingly.[22]

To test the reproducibility of this label-free impedance DNA hybridization sensing, four parallel immobilizations of 1.0×10^{-6} M hpDNA on the Au-PDI-graphene modified GCE were performed and then hybridized with 1.0×10^{-10} M cDNA, respectively. The ΔR_{et} values before and after hybridization were calculated to be 2250, 2000, 2175 and 2300 Ω, respectively. Their relative standard deviation (RSD) was estimated to be 6.03%, confirming the high reproducibility of the DNA hybridization detection platform.

The good stability of hpDNA platform was contributed to excellent sensitivity. And the stability of the hpDNA captured platform was tested at 37 ℃ by incubating the electrode in ultrapure water, Tris–HCl solution, 2 × SSC solution, respectively. After incubation for 6 hours, the EIS of the electrode retained almost the same, demonstrating good stability of the DNA hybridization detection platform.

Conclusions

In summary we have introduced a bifunctional PDI molecule to act as dispersion reagent and a linker to densely graft nanoparticles on graphene. The as-prepared PDI-graphene nanohybrid exhibits high stability and sufficiently nanoparticle loading ability. Moreover, we performed a comprehensive study of the fundamental electrochemical properties of the Au-PDI-graphene modified electrode interface and explored the biological sensor application. The fabricated hpDNA biosensor displays a sensitive electrochemical impedance response to HIV-1 gene and shows a wide linear detection range and a relatively low detection limit. This efficient electrochemical impedance sensitivity suggests potentially specific applications in biodiagnostics and bionanotechnology.

Acknowledgements

The authors are most grateful to the NSFC (No. 21205112, 21105096, 21175130 and 21225524) , Ministry of Science and Technology of China (2012YQ170003) and Department of Science and Technology of Jilin Province (No. 201215091 and 20120308).

Notes and references

Engineering Laboratory for Modern Analytical Techniques, c/oState Key Laboratory of Electroanalytical Chemistry, Changchun Institute of applied Chemistry, Chinese Academy of Sciences, Changchun 30022, PR China. Fax: +8643185262800; Tel: +8643185262425; E-mail: lniu@ciac.ac.cn, jhli@ciac.ac.cn.

† Electronic Supplementary Information (ESI) available: Materials; Apparatus and characterization; FTIR spectrum of PDI molecule; TableS1† The characteristic peaks of GO, graphene, PDI and PDI-graphene; XPS spectra of GO and graphene, the Au4f of AuNPs on Au-PDI-graphene; Table S2† Comparison of the proposed platform with others for specific DNA sequence hybridization detection using EIS.

1. X. Liu, R. Aizen, R. Freeman, O. Yehezkeli and I. Willner, *ACS Nano*, 2012, **6**, 3553.
2. L. Zhang, J. Xia, Q. Zhao, L. Liu and Z. Zhang, *Small*, 2010, **6**, 537.
3. A. Sahu, W. I. Choi, J. H. Lee and G. Tae, *Biomaterials*, 2013, **34**, 6239.
4. C.-T. Lin, P. T. K. Loan, T.-Y. Chen, K.-K. Liu, C.-H. Chen, K.-H. Wei and L.-J. Li, *Adv. Funct. Mater.*, 2013, **23**, 2301.
5. J. C. Claussen, A. Kumar, D. B. Jaroch, M. H. Khawaja, A. B. Hibbard, D. M. Porterfield and T. S. Fisher, *Adv. Funct. Mater.*, 2012, **22**, 3399.
6. S. Park and R. S. Ruoff, *Nat Nano*, 2010, **5**, 309.
7. R. Muszynski, B. Seger and P. V. Kamat, *J. Phys. Chem. C*, 2008, **112**, 5263.
8. (a) Q. Yue, K. Zhang, X. Chen, L. Wang, J. Zhao, J. Liu and J. Jia, *Chem. Commun.*, 2010, **46**, 3369; (b) B. Cai, X. Lv, S. Gan, M. Zhou, W. Ma, T. Wu, F. Li, D. Han and L. Niu, *Nanoscale*, 2013, **5**, 1910.
9. (a) S. Sun and P. Wu, *Phys. Chem. Chem. Phys.*, 2011, **13**, 21116; (b) J. Tian, S. Liu, Y. Zhang, H. Li, L. Wang, Y. Luo, A. M. Asiri, A. O. Al-Youbi and X. Sun, *Inorg. Chem.*, 2012, **51**, 4742.
10. X. Qi, K.-Y. Pu, H. Li, X. Zhou, S. Wu, Q.-L. Fan, B. Liu, F. Boey, W. Huang and H. Zhang, *Angew. Chem.-Int. Edit.*, 2010, **49**, 9426.
11. (a) J. Shen, Y. Hu, C. Li, C. Qin and M. Ye, *Small*, 2009, **5**, 82; (b) H. Yang, C. Shan, F. Li, D. Han, Q. Zhang and L. Niu, *Chem. Commun.*, 2009, 3880.
12. (a) W. S. Hummers and R. E. Offeman, *J. Am. Chem. Soc.*, 1958, **80**, 1339; (b) N. I. Kovtyukhova, P. J. Ollivier, B. R. Martin, T. E. Mallouk, S. A. Chizhik, E. V. Buzaneva and A. D. Gorchinskiy, *Chem. Mater.*, 1999, **11**, 771.
13. Y. Hu, K. Wang, Q. Zhang, F. Li, T. Wu and L. Niu, *Biomaterials*, 2012, **33**, 1097.
14. J. Gao, C. M. Bender and C. J. Murphy, *Langmuir*, 2003, **19**, 9065.
15. D. Li, M. B. Muller, S. Gilje, R. B. Kaner and G. G. Wallace, *Nat. Nanotechnol.*, 2008, **3**, 101.
16. (a) A. D. Q. Li, W. Wang and L.-Q. Wang, *Chem. Eur. J.*, 2003, **9**, 4594; (b) C. Backes, C. D. Schmidt, K. Rosenlehner, F. Hauke, J. N. Coleman and A. Hirsch, *Adv. Mater.*, 2010, **22**, 788.

17. C. Backes, C. D. Schmidt, F. Hauke, C. Böttcher and A. Hirsch, *J. Am. Chem. Soc.*, 2009, **131**, 2172.
18. F. Li, H. Yang, C. Shan, Q. Zhang, D. Han, A. Ivaska and L. Niu, *J. Mater. Chem.*, 2009, **19**, 4022.
19. (a) A. P. R. Johnston, A. N. Zelikin, L. Lee and F. Caruso, *Anal. Chem.*, 2006, **78**, 5913; (b) Z. Wang, Q. Zhang, D. Kuehner, X. Xu, A. Ivaska and L. Niu, *Carbon*, 2008, **46**, 1687.
20. P. Diao, M. Guo and Q. Zhang, *J. Phys. Chem. C*, 2008, **112**, 7036.
21. (a) Y. Hu, F. Li, D. Han, T. Wu, Q. Zhang, L. Niu and Y. Bao, *Anal. Chim. Acta*, 2012, **753**, 82; (b) W. Zhang, P. Zong, X. Zheng and L. Wang, *Biosens. Bioelectron.*, 2013, **42**, 481; (c) Y. Wang, C. Li, X. Li, Y. Li and H.-B. Kraatz, *Anal. Chem.*, 2008, **80**, 2255.
22. T. H. M. Kjällman, H. Peng, C. Soeller and J. Travas-Sejdic, *Anal. Chem.*, 2008, **80**, 9460.
23. (a) H. Du, M. D. Disney, B. L. Miller and T. D. Krauss, *J. Am. Chem. Soc.*, 2003, **125**, 4012; (b) S. Tyagi and F. R. Kramer, *Nat. Biotechnol.*, 1996, **14**, 303; (c) H. Du, C. M. Strohsahl, J. Camera, B. L. Miller and T. D. Krauss, *J. Am. Chem. Soc.*, 2005, **127**, 7932; (d) Y. Xu, L. Yang, X. Ye, P. He and Y. Fang, *Electroanal.*, 2006, **18**, 873; (e) X. Fang, X. Liu, S. Schuster and W. Tan, *J. Am. Chem. Soc.*, 1999, **121**, 2921.